

APPLICATION OF THE ROTATION MATRIX NATURAL INVARIANTS TO IMPEDANCE CONTROL OF ROTATIONAL PARALLEL ROBOTS

L. Bruzzone¹, M. Callegari²

ABSTRACT

Force control of parallel robots with rotational degrees of freedom through impedance algorithms is considerably influenced by the representation method of the end-effector orientation. Using the natural invariants of the rotation matrix and the angular velocity vector in the impedance control law has some theoretical advantages, which derive from the Euclidean-geometric meaning of these entities. These benefits are particularly evident in case of robotic architectures with three rotational degrees of freedom (serial or parallel wrists with spherical motion). The behaviour of a 3-CPU parallel robot controlled by an impedance algorithm based on this concepts is assessed through multibody simulations, and the results confirm the effectiveness of the proposed approach.

KEYWORDS

Parallel robots, natural invariants of the rotation matrix, impedance control

1. INTRODUCTION

Several robotic applications involve the control of the interaction forces between end-effector and external environment; the control laws that can fulfil this requirement can be divided into two families: hybrid position/force control algorithms and impedance control algorithms. These two approaches have been widely discussed and compared in the scientific literature during the last decades, in particular with reference to serial kinematics [1-5].

In the last years the industrial interest about parallel robots (parallel kinematics machines, PKMs) is growing; mass-produced parallel manipulators are widely used especially in two categories of applications:

¹ PMAR Robot Design Research Group - DIMEC - University of Genova, Genova, Italy, corresponding author

² Department of Mechanics, Polytechnic University of Marche, Ancona, Italy

- fast speed pick-and-place tasks with small payloads; in this case high-speed, lightweight parallel robots are adopted for their excellent dynamic performances, due to the low moving masses (for example the FlexPicker IRB340 by ABB based on the Delta kinematics [6]);
- machining or assembly tasks characterized by high forces, which requires high structural stiffness and positioning accuracy; in this case high-stiffness PKMs (for example the F-200iB by Fanuc based on the Gough-Stewart kinematics [7, 8] or the Tricept by Neos Robotics AB) [9]) offer a high ratio between maximum payload/force and robot mass.

In most cases, parallel robots are position-controlled; nevertheless, the scientific and industrial interest about force-controlled PKMs is growing, even if only a few works on the subject are presently available, probably due to the fact that PKM's are relatively new architectures, characterised by quite complex kinematic and dynamic models [10-12]. In particular, the use of impedance-controlled parallel robots [13-16] is an effective solution: the moving masses of PKMs are limited, because the actuators are usually fixed to the ground, then it is possible to realise the desired stiffness-damping behaviour neglecting the compensations of the inertial terms.

One of the major problems in the synthesis of a suitable impedance control law (both for serial and parallel robots) is the definition of the rotational stiffness, which is strictly related to the representation method for the end-effector orientation [17]. While the position of a point in space can be easily defined by a three-dimensional vector, there are many mathematical tools to represent the orientation of a rigid body in space [18, 19] and this influences the resulting impedance control law. In the following of the paper this aspect will be discussed with reference to simulation results involving an impedance-controlled 3-CPU parallel robotic wrist.

2. REPRESENTATION OF THE END-EFFECTOR ORIENTATION

Probably, the most common method to describe the orientation of a rigid body is the use of the Euler angles; nevertheless, this method has many drawbacks [20, 21]:

- there are 12 different sets of Euler angles, and the choice of a set influences arbitrarily the control algorithm;

- there are representation singularities (configurations defined by non-unique values of Euler angles), and in these singularity loci it is impossible to describe an arbitrary angular velocity as function of the Euler angles time derivatives.

Some researchers tried to overcome these limitations by using a modified set of Euler angles that avoid singularities [22] or the so-called Euler parameters, a 4-dimensional vector of invariants that are not geometric entities [23].

Another possible representation of the orientation is the 3x3 rotation matrix, but its nine elements are not independent and an impedance algorithm based on three independent rotation matrix elements is poor of geometrical meaning.

An arbitrary rigid body rotation is uniquely defined by the *axis of rotation* (represented by the unit vector \mathbf{e}) and the *angle of rotation* θ , which is the amount of rotation according to the right-hand rule; the unit vector \mathbf{e} and the angle θ are the *natural invariants* of the rotation matrix, independent from the reference frame [18].

In [24] the use of the frame-invariant vector $\mathbf{E} = \theta\mathbf{e}$ in the impedance control law is proposed. The main advantage of the use of this vector is related to its geometrical meaning and strict relation to the angular velocity vector $\boldsymbol{\omega}$:

$$\boldsymbol{\omega} = \sin \theta \dot{\mathbf{e}} + (1 - \cos \theta) \mathbf{e} \times \dot{\mathbf{e}} + \theta \dot{\mathbf{e}} \quad (1)$$

In an impedance algorithm the vector \mathbf{E} can be used to represent the rotation between the actual end-effector orientation and the reference orientation; in this case the maximum values of θ are limited. It is easy to demonstrate that if θ tends to zero, the angular velocity vector tends to the time derivative of \mathbf{E} :

$$\lim_{\theta \rightarrow 0} \boldsymbol{\omega} = \theta \dot{\mathbf{e}} + \dot{\theta} \mathbf{e} = \frac{d}{dt} \mathbf{E} \quad (2)$$

This is a very important propriety of the vector \mathbf{E} , because an impedance control law based on the vector \mathbf{E} for the stiffness term and on the angular velocity vector $\boldsymbol{\omega}$ for the damping term uses two vectors that are nearly in relation of time derivative. This important propriety is not shared by the other orientation

representation methods, and it leads to a more natural and intuitive robot behaviour. The advantages of such an approach in case of a six-degree-of-freedom parallel robot are shown in [24]; in case of a purely rotational three-degree-of-freedom parallel robot the benefits are even more evident, and this will be shown in the following of the paper.

3. THE 3-CPU PARALLEL ARCHITECTURE

In the 3-CPU architecture [25] (Fig. 1) three identical serial chains (legs) connect the fixed base and the rotating end-effector platform; each leg (Fig. 2) is composed of two links; the first link is connected to the base by a cylindrical joint and to the second link by a prismatic joint; the second link is connected to the end-effector by a universal joint.

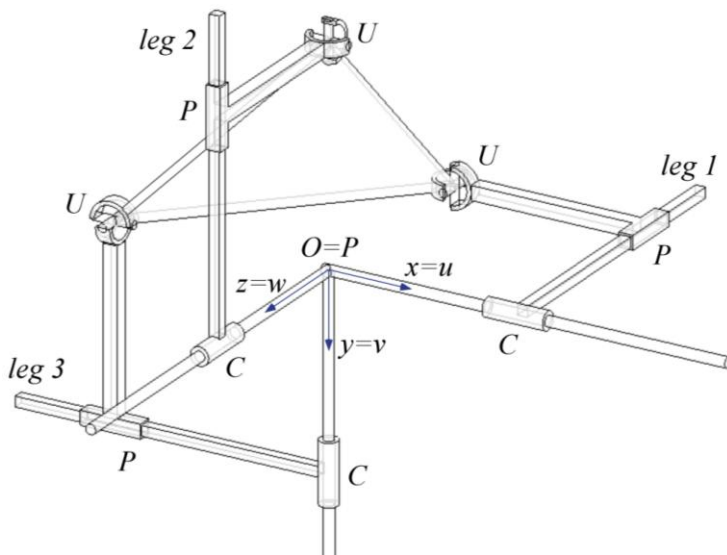


Fig. 1 – the 3-CPU parallel architecture

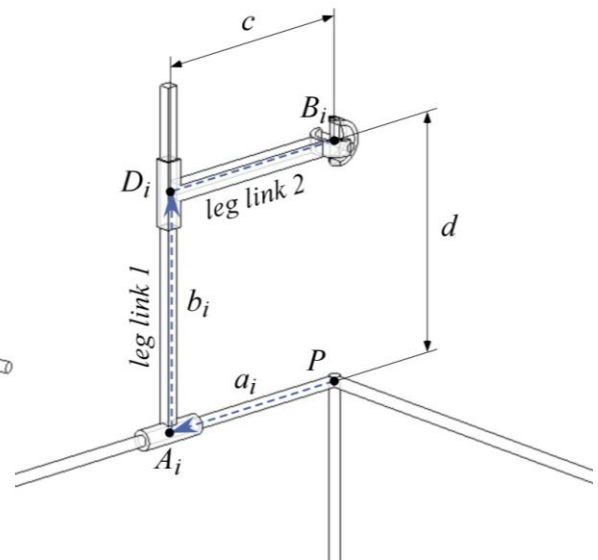


Fig. 2 – leg of the CPU parallel architecture

The axes of the cylindrical joints $\overset{v}{\mathbf{a}}_i$, $i=1,2,3$, intersect at the *centre of motion* O and are aligned to the x,y,z axes of the fixed reference frame, with its centre in O . The first link of i -th leg is perpendicular to the axis $\overset{v}{\mathbf{a}}_i$, and has a variable length b_i thanks to the prismatic joint D_i ; the second link is parallel to $\overset{v}{\mathbf{a}}_i$. The first axis of the universal joint B_i is perpendicular to the plane of the i -th leg, while the second axis intersects at the point P the corresponding axes of the other legs; these three axes are coincident to the v,w,u axes of a

cartesian frame located in P and attached to the end-effector. If proper *manufacturing* and *mounting conditions* are fulfilled the centres of the fixed frame $O(x,y,z)$ and rotating frame $P(u,v,w)$ remain coincident during the motion, and the end-effector performs a spherical motion. In particular, in the initial configuration the three linear displacements a_i of the cylindrical joints are equal to c and the linear displacements b_i of the prismatic joints are equal to d (Fig. 2). The spherical motion of the end-effector can be driven by actuating the linear displacements of the cylindrical joints; therefore, the vector of the internal coordinates is:

$$\mathbf{q} = \begin{bmatrix} a_1 \\ a_2 \\ a_3 \end{bmatrix} \quad (3)$$

The direct and inverse kinematics of the robot make the forward and backward connections between the internal coordinates and the relative rotation of the frame $P(u,v,w)$ with respect to $O(x,y,z)$.

The choice of the three external coordinates influences the impedance control law; in the following, two possible sets of external coordinates are considered:

- the set of Euler angles α, β, γ corresponding to three subsequent rotations along the axes u, v, w that represent the overall relative rotation between $O(x,y,z)$ and $P(u,v,w)$;
- the three components of the vector ${}^o_p \mathbf{E}$ that represent the overall relative rotation between $O(x,y,z)$ and $P(u,v,w)$.

Independently of the selected set of external coordinates, the direct kinematic problem admits up to 8 solutions, while the solution of the inverse kinematics is single [25]. The choice of the external coordinates determines the consequent Jacobian matrix: deriving the two possible sets of inverse kinematics equations, two alternative analytical Jacobian matrices can be found:

- the analytical Jacobian matrix \mathbf{J}_A , which relates the time derivative of \mathbf{q} and the time derivatives of the Euler angles, collected in the vector α_p :

$$\frac{d}{dt} \mathbf{q} = \mathbf{J}_A \begin{bmatrix} \dot{\alpha} \\ \dot{\beta} \\ \dot{\gamma} \end{bmatrix} = \mathbf{J}_A \frac{d}{dt} \alpha_p \quad (4)$$

- the analytical Jacobian matrix \mathbf{J}_E , which relates the time derivative of \mathbf{q} and the time derivative of \mathbf{E} :

$$\frac{d}{dt} \mathbf{q} = \mathbf{J}_E \frac{d}{dt} {}^o_P \mathbf{E} \quad (5)$$

The geometric Jacobian \mathbf{J}_G represents the relationship between the time derivative of \mathbf{q} and the end-effector angular velocity vector $\boldsymbol{\omega}_P$:

$$\frac{d}{dt} \mathbf{q} = \mathbf{J}_G \boldsymbol{\omega}_P \quad (6)$$

It is easy to demonstrate, by using the equations (2), (5) and (6), that if θ tends to zero, the Jacobian matrices \mathbf{J}_G and \mathbf{J}_A tends to be equal:

$$\lim_{\theta \rightarrow 0} \mathbf{J}_G = \lim_{\theta \rightarrow 0} \mathbf{J}_E \quad (7)$$

4. IMPEDANCE CONTROL ALGORITHM

The basic concept of impedance control is that the robot end-effector, subject to external forces, follows a trajectory with a predetermined spatial compliance [26, 27]; this compliance, which influences the end-effector dynamic behaviour, is defined by the *stiffness matrix* \mathbf{K} and the *damping matrix* \mathbf{C} ; the reference configuration of the end-effector is a *virtual equilibrium state* because it corresponds to an actual equilibrium only if no force is exerted by the environment.

The actual position of the end-effector can be represented alternatively by the external coordinates vectors $\boldsymbol{\alpha}_P$ or ${}^o_P \mathbf{E}$; similarly, the virtual equilibrium configuration, corresponding to the reference frame D , can be represented by the Euler angles $\boldsymbol{\alpha}_D$ or by the vector ${}^o_D \mathbf{E}$. Using the principle of the virtual work and considering the equations (4), (5) and (7), the two impedance control laws (8) and (10) can be derived, the first based on the Euler angles and the analytical Jacobian matrix \mathbf{J}_A , the second based on the vector \mathbf{E} and the geometric Jacobian matrix \mathbf{J}_G :

$$\mathbf{F} = \mathbf{J}_A^T {}^{-1} \left[\mathbf{K}_r \boldsymbol{\alpha}_D - \boldsymbol{\alpha}_P + \mathbf{C}_r \boldsymbol{\omega}_D - \boldsymbol{\omega}_P \right] \quad (8)$$

where [25]:

$$\mathbf{J}_A = d \begin{bmatrix} 0 & -s\beta s\gamma & c\beta c\gamma \\ c\alpha c\beta & -s\alpha s\beta & 0 \\ -s\alpha s\beta c\gamma - c\alpha s\gamma & c\alpha c\beta c\gamma & -c\alpha s\beta s\gamma - s\alpha c\gamma \end{bmatrix} \quad (9)$$

$$\mathbf{F} = \mathbf{J}_G^T \mathbf{J}_G^{-1} \left[\mathbf{K}_r \mathbf{E} - \mathbf{C}_r \dot{\mathbf{E}} + \mathbf{C}_r \boldsymbol{\omega}_D - \boldsymbol{\omega}_P \right] \quad (10)$$

where [25]:

$$\mathbf{J}_G = d \begin{bmatrix} 0 & -c\alpha s\beta s\gamma - s\alpha c\gamma & c\alpha c\gamma - s\alpha s\beta s\gamma \\ c\alpha c\beta & 0 & -s\beta \\ -s\alpha s\beta c\gamma - c\alpha c\beta s\gamma & c\beta c\gamma & 0 \end{bmatrix} \quad (11)$$

In the control laws (8) and (10):

- \mathbf{F} is the vector of the three actuation forces, acting along the axes of the cylindrical joints;
- \mathbf{K}_r is the *rotational stiffness matrix*, which expresses the relation between rotation and elastic torque in the desired impedance control behaviour;
- \mathbf{C}_r is the *rotational damping matrix*, which expresses the relation between rate of rotation and viscous torque in the desired impedance control behaviour.

Let us note that in the control law (10) the damping term is not based on the derivatives of the external coordinates, but on the angular velocity vector. The matrices \mathbf{K}_r and \mathbf{C}_r are in general non-diagonal; it is possible to define \mathbf{K}_r and \mathbf{C}_r using a principal reference frame (*PR*) in which they are diagonal; this principal reference frame can be selected on the basis of the task requirements; it is possible to obtain \mathbf{K}_r and \mathbf{C}_r in the world frame (*O*) by means of the rotation matrix ${}^{PR}_O \mathbf{R}$ [24]:

$$\mathbf{K}_r = {}^{PR}_O \mathbf{R}^T {}^{PR} \mathbf{K}_r {}^{PR}_O \mathbf{R} = {}^{O}_{PR} \mathbf{R} {}^{PR} \mathbf{K}_r {}^{O}_{PR} \mathbf{R}^T \quad (12)$$

$$\mathbf{C}_r = {}^{PR}_O \mathbf{R}^T {}^{PR} \mathbf{C}_r {}^{PR}_O \mathbf{R} = {}^{O}_{PR} \mathbf{R} {}^{PR} \mathbf{C}_r {}^{O}_{PR} \mathbf{R}^T \quad (13)$$

where ${}^{PR} \mathbf{K}_r$ and ${}^{PR} \mathbf{C}_r$ are the stiffness and damping matrices expressed in the principal reference frame.

In the following section, the control laws (8) and (10) will be compared by means of multibody simulation, to show the advantages of the second control law, due to the geometric properties of the vector \mathbf{E} .

5. SIMULATION RESULTS

The impedance control laws (8) and (10) have been applied to a 3-CPU parallel robot with the geometric and inertial parameters shown in Table 1. Since the two links of each leg rotate only about the corresponding cylindrical joint axis, only the moments of inertia with respect to this direction are reported; the universal joints crosses can be considered lumped masses concentrated in the corresponding universal joint centres.

<i>geometric parameters</i>	
<i>c</i>	93.5 mm
<i>d</i>	106.07 mm
<i>main inertial parameters</i>	
<i>end-effector mass</i>	$3.893 \cdot 10^{-1}$ kg
<i>end effector inertia matrix with respect to the coordinate frame $P(u,v,w)$</i>	$\begin{bmatrix} 1.426 & -0.356 & -0.356 \\ -0.356 & 1.426 & -0.356 \\ -0.356 & -0.356 & 1.426 \end{bmatrix} \cdot 10^{-3} \text{ kgm}^2$
<i>mass of the leg link 1</i>	$3.944 \cdot 10^{-2}$ kg
<i>moment of inertia of the leg link 1 about its cylindrical joint axis</i>	$2.364 \cdot 10^{-4}$ kgm ²
<i>mass of the leg link 2</i>	$3.928 \cdot 10^{-2}$ kg
<i>moment of inertia of the leg link 2 about its principal axis parallel to the cylindrical joint axis of the same leg</i>	$8.447 \cdot 10^{-7}$ kgm ²
<i>mass of the universal joint cross</i>	$3.59 \cdot 10^{-3}$ kg

Table 1 – geometric and inertial properties of the considered 3-CPU mechanism

Case study A

In the case study A, starting from the initial condition with the coordinate frames P and O coincident, a moment ${}^O\mathbf{M}$ with direction $[-1,1,0.5]^T$ and magnitude 20 Nmm is applied to the end-effector. The control system imposes an isotropic rotational behaviour, defined by the following diagonal stiffness and damping matrices:

$${}^{PR}\mathbf{K}_r = \mathbf{K}_r = \begin{bmatrix} 100 & 0 & 0 \\ 0 & 100 & 0 \\ 0 & 0 & 100 \end{bmatrix} \text{ Nmm/rad} \quad (14)$$

$${}^{PR}\mathbf{C}_r = \mathbf{C}_r = \begin{bmatrix} 16.88 & 0 & 0 \\ 0 & 16.88 & 0 \\ 0 & 0 & 16.88 \end{bmatrix} \text{ Nmms/rad} \quad (15)$$

The value of the desired isotropic stiffness ($k=100$ Nmm/rad) is arbitrary; the value of the isotropic damping coefficient is selected using an heuristic approach, considering each rotational direction as a linear inertia-torsional spring-torsional damper system with a damping coefficient $\xi = \sqrt{2}/2$. Therefore, the following well-known formula is used:

$$c = 2 \xi \sqrt{k J} \quad (16)$$

where $J = 1.426 \cdot 10^{-3} \text{ kgm}^2 = 1.426 \text{ Ns}^2/\text{mm}$ is the end-effector moment of inertia (Table 1).

The rotational behaviour of the robot about the three directions can be compared with three decoupled second-order inertia-rotational spring-rotational damper systems, characterized by the following linear differential equations:

$$\begin{aligned} 3.10 \ddot{\varphi}_x + 16.88 \dot{\varphi}_x + 100 \varphi_x &= -13.33 \\ 3.10 \ddot{\varphi}_y + 16.88 \dot{\varphi}_y + 100 \varphi_y &= 13.33 \\ 3.10 \ddot{\varphi}_z + 16.88 \dot{\varphi}_z + 100 \varphi_z &= 6.67 \end{aligned} \quad (17)$$

For these three decoupled systems:

- the inertia of $3.10 \cdot 10^{-3} \text{ kgm}^2 = 3.10 \text{ Ns}^2/\text{mm}$ derives from the end-effector moment of inertia increased considering approximately the leg links 1 and 2 as lumped masses placed respectively at a distance of $d/2$ and d from the point O ;
- the stiffness and damping coefficients are equal to the isotropic stiffness and damping coefficients k and c ;
- the applied moments are the three components of the moment ${}^O\mathbf{M}$.

Figures 3 to 5 show the rotational behaviour of the robot controlled by the law (8), based on the analytical Jacobian matrix, in comparison with the three decoupled systems (17); in these graphs the end-effector orientation is represented both by the components of the vector ${}^o_p\mathbf{E}$ and by the Euler angles; figures 6 to 8 refer to the rotational behaviour of the robot controlled by the law (10), based on the geometric Jacobian matrix.

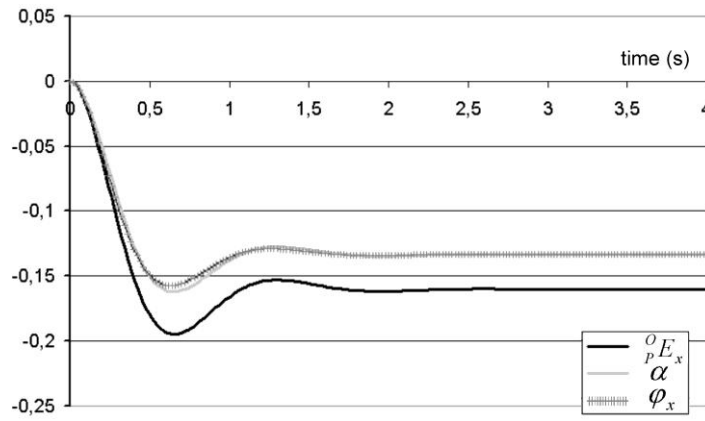


Fig. 3 – comparison of ${}^o_p E_x$, α and φ_x with the control law (8) in the case study A

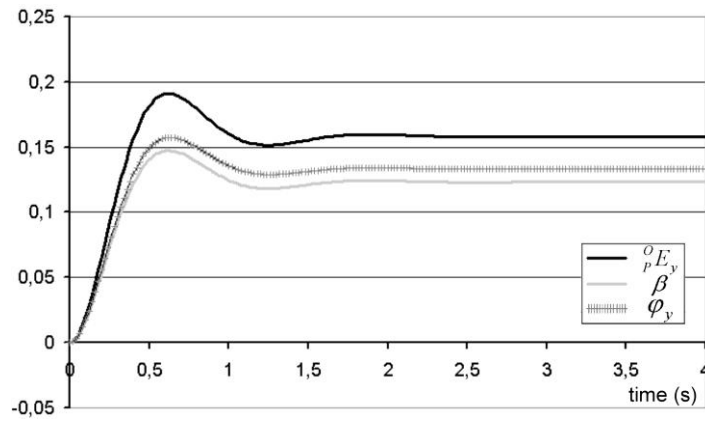


Fig. 4 – comparison of ${}^o_p E_y$, β and φ_y with the control law (8) in the case study A

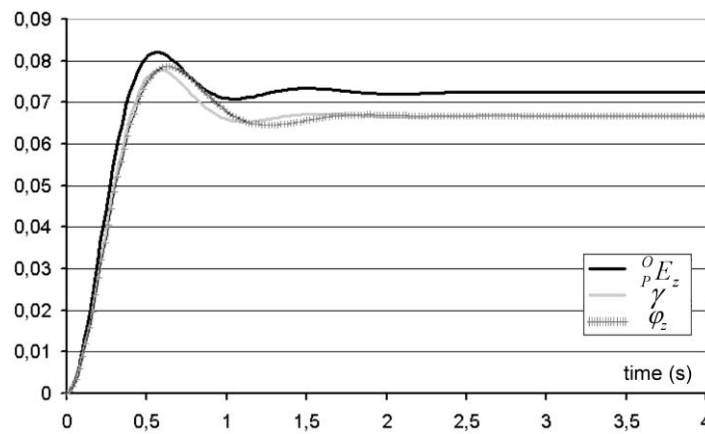


Fig. 5 – comparison of ${}^o_p E_z$, γ and φ_z with the control law (8) in the case study A

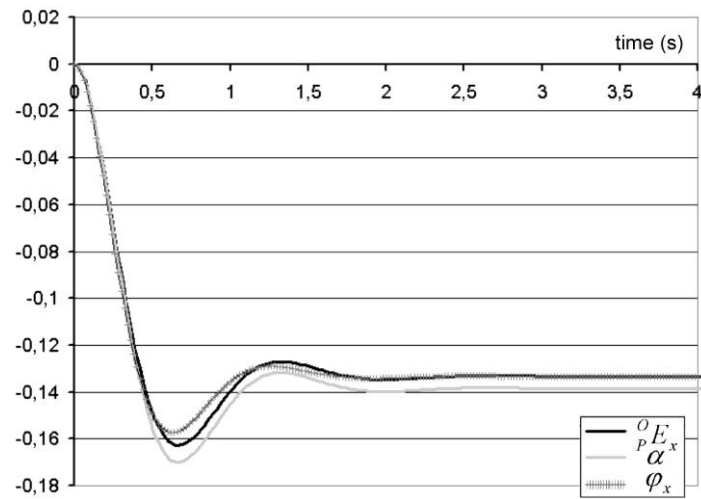


Fig. 6 – comparison of $^o_P E_x$, α and φ_x with the control law (10) in the case study A

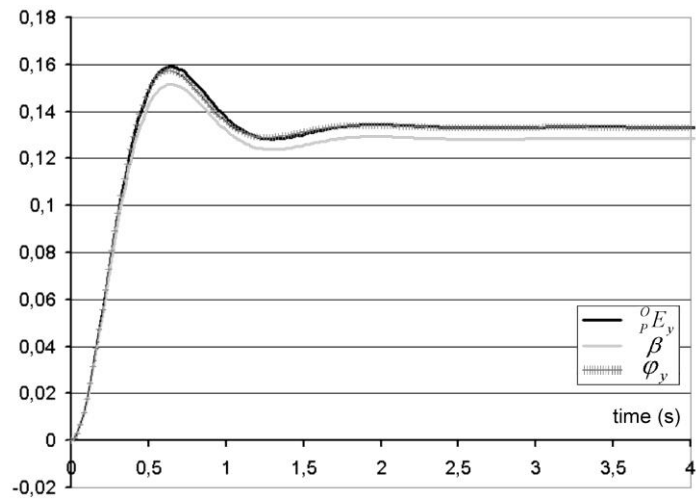


Fig. 7 – comparison of $^o_P E_y$, β and φ_y with the control law (10) in the case study A

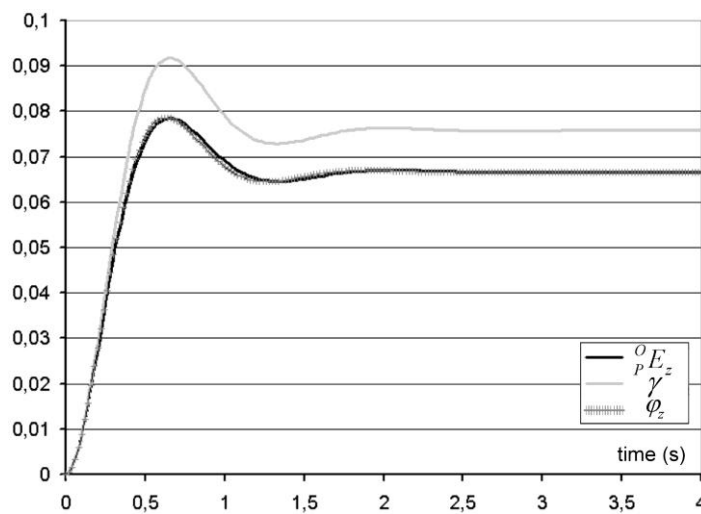


Fig. 8 – comparison of $^o_P E_z$, γ and φ_z with the control law (10) in the case study A

Both the control laws apply the isotropic stiffness and damping expressed by the matrices (14) and (15), but only the geometric control law (10) realizes an isotropic behaviour: in final steady state the end-effector rotation is ${}^o_p\mathbf{E} = -0.1333, 0.1333, 0.0667^T$ rad, that is a rotation with the same direction of the external moment ${}^o\mathbf{M}$ and magnitude equal to the magnitude of ${}^o\mathbf{M}$ divided by the isotropic stiffness k . On the contrary, using the analytical control law (8) the final rotation is ${}^o_p\mathbf{E} = -0.1601, 0.1582, 0.0724^T$ rad. Moreover, it is possible to note that using the geometric control law (10) the time histories of the three components of ${}^o_p\mathbf{E}$ are very similar to the ones of the three decoupled linear systems; this means that the rotational behaviour of the robot is very intuitive and almost decoupled in the three directions.

Case study B

In the case study B, starting from the initial condition with the coordinate frames P and O coincident, a moment ${}^o\mathbf{M}$ with direction $[-1, 0, 1]^T$ and magnitude 20 Nmm is applied to the end-effector. Now the control system imposes a non-isotropic rotational behaviour; the stiffness and damping matrices are defined in a principal reference frame PR , which is rotated with respect to O according to the following vector \mathbf{E} :

$${}^{PR}_o\mathbf{E} = \begin{bmatrix} \frac{1}{\sqrt{3}} & \frac{1}{\sqrt{3}} & \frac{1}{\sqrt{3}} \end{bmatrix}^T \quad (18)$$

which corresponds to the rotation matrix:

$${}^{PR}_o\mathbf{R} = \begin{bmatrix} 0.6935 & -0.3326 & 0.6391 \\ 0.6391 & 0.6935 & -0.3326 \\ -0.3326 & 0.6391 & 0.6935 \end{bmatrix} \quad (19)$$

The principal rotational stiffness and damping matrices are:

$${}^{PR}\mathbf{K}_r = \begin{bmatrix} 50 & 0 & 0 \\ 0 & 1000 & 0 \\ 0 & 0 & 1000 \end{bmatrix} \text{ Nmm/rad} \quad (20)$$

$${}^{PR}\mathbf{C}_r = \begin{bmatrix} 11.94 & 0 & 0 \\ 0 & 53.4 & 0 \\ 0 & 0 & 53.4 \end{bmatrix} \text{ Nmms/rad} \quad (21)$$

The matrix ${}^{PR}\mathbf{K}_r$ imposes a rotational stiffness about the first principal axis much lower than about the other two axes, in order to have large rotations only in one direction and negligible rotations in the other two directions, independently of the direction of the applied moment; the diagonal values of ${}^{PR}\mathbf{C}_r$ are obtained by the formula (16) as in the previous case study. The rotational stiffness and damping matrices in the reference frame O can be obtained by the equations (12) and (13).

The rotational behaviour of the robot about the three principal directions is compared with three decoupled second-order inertia-rotational spring-rotational damper systems loaded by the components of the external

$$\text{moment } {}^{PR}\mathbf{M} = {}^{PR}\mathbf{R}_o^O \mathbf{M} = \begin{bmatrix} -14.51 & 13.74 & 0.769 \end{bmatrix}^T :$$

$$\begin{aligned} 3.10 \ddot{\varphi}_x + 11.94 \dot{\varphi}_x + 50 \varphi_x &= -14.51 \\ 3.10 \ddot{\varphi}_y + 53.4 \dot{\varphi}_y + 1000 \varphi_y &= 13.74 \\ 3.10 \ddot{\varphi}_z + 53.4 \dot{\varphi}_z + 1000 \varphi_z &= 0.769 \end{aligned} \quad (22)$$

Figures 9 to 11 show the behaviour of the robot controlled by the law (8), based on the analytical Jacobian matrix, in comparison with the three decoupled systems (22); figures 12 to 14 show the same comparison, but applying the law (10), based on the geometric Jacobian matrix. In these graphs the end-effector orientation with respect to the principal stiffness and damping reference frame is represented both by the components of the vector ${}^{PR}\mathbf{E} = {}^{PR}\mathbf{R}_o^O \mathbf{E}$ and by the Euler angles.

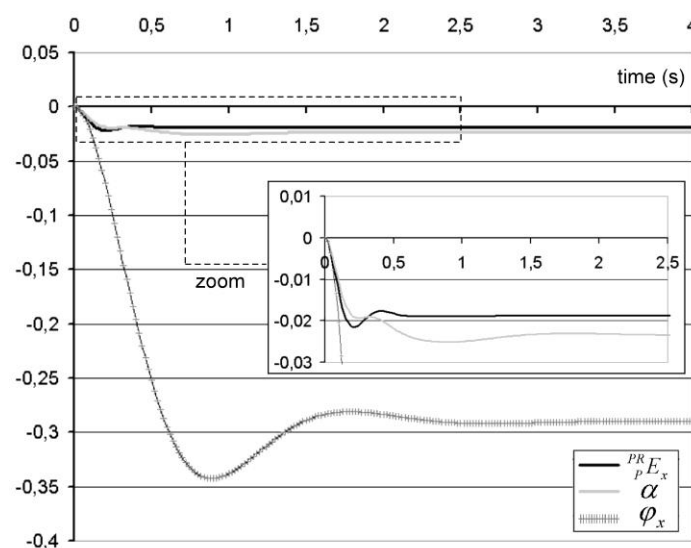


Fig. 9 – comparison of ${}^o P E_x$, α and φ_x with the control law (8) in the case study B

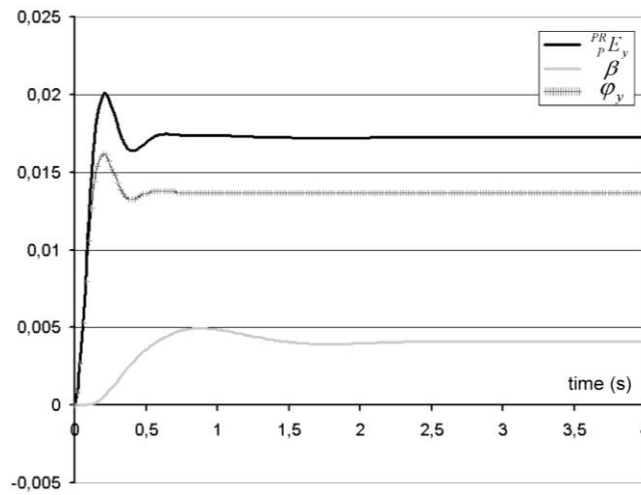


Fig. 10 – comparison of ${}^o P E_y$, β and φ_y with the control law (8) in the case study B

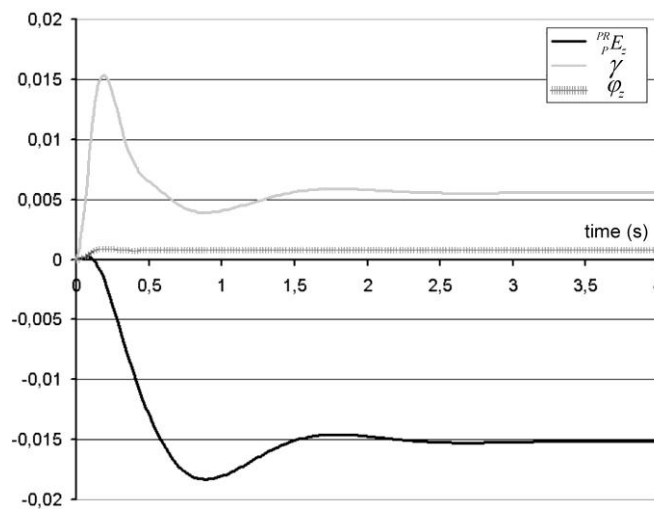


Fig. 11 – comparison of ${}^o P E_z$, γ and φ_z with the control law (8) in the case study B

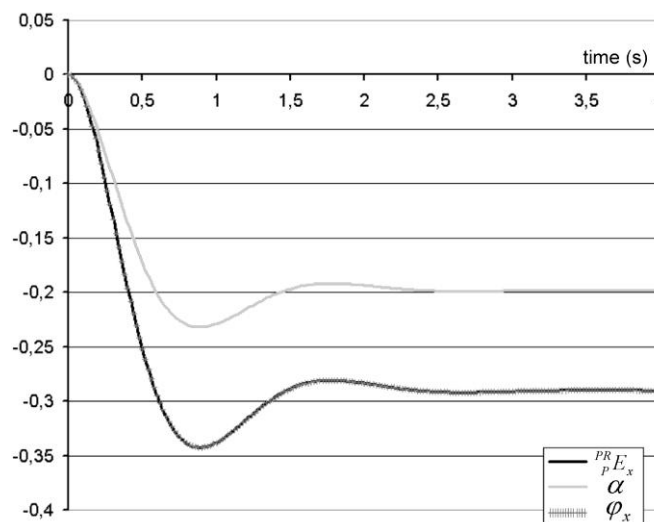


Fig. 12 – comparison of ${}^P E_x$, α and φ_x with the control law (10) in the case study B

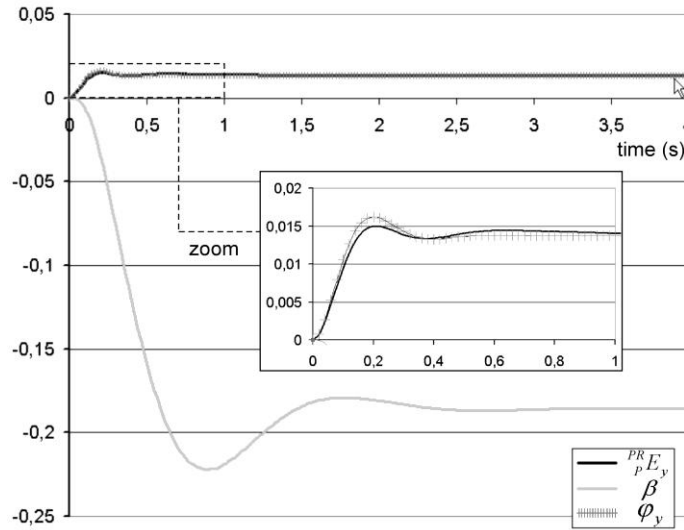


Fig. 13 – comparison of ${}^p E_y$, β and φ_y with the control law (10) in the case study B

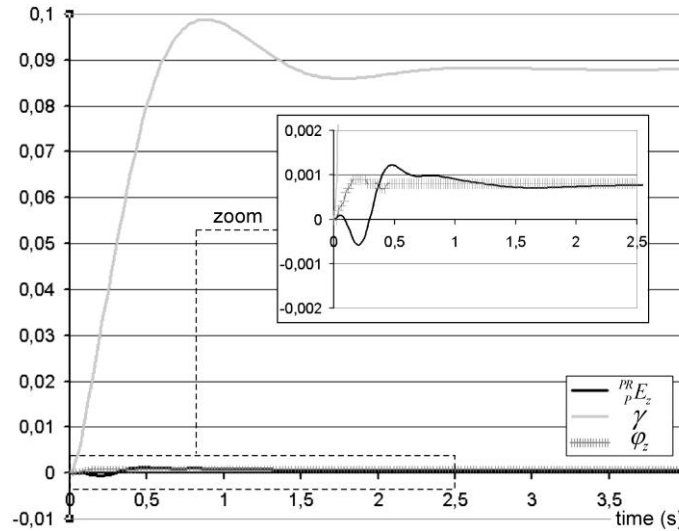


Fig. 14 – comparison of ${}^p E_z$, γ and φ_z with the control law (10) in the case study B

It is possible to note that using the control law (8) the rotational behaviour of the robot is remarkably different from the decoupled systems; on the contrary, using the control law (10) the time histories of the three components of the vector ${}^p \mathbf{E}$ are very close to the ones of the three decoupled systems:

- the relative difference between ${}^p E_x$ and φ_x , after 0.5s, remains lower than 0.15% (Fig. 12); this rotation direction is the most significant because it is the one with higher compliance;

- the relative difference between ${}^P E_y$ and φ_y has a peak of 9.8% at 0.2s (zoom box of Fig. 13) but rapidly decreases;
- the relative difference between ${}^P E_z$ and φ_z is high only in the first second (zoom box of Fig. 14).

All the relative differences tends to zero in steady state. These results show that the control law (10) imposes successfully the rotational compliance about the three principal axes, and is capable of effectively constrain the rotation direction; the robot behaviour is almost decoupled in the three rotation directions and similar to a linear three-degree-of-freedom second-order system. Let us note that complete decoupling of the robot dynamic behaviour could be obtained by introducing the model-based compensation of the inertial terms [28], but this increases remarkably the computational burden without significant benefits.

6. CONCLUSIONS

The vector $\mathbf{E} = \theta \mathbf{e}$ is the product of the unit vector \mathbf{e} representing the *axis of rotation* and the *angle of rotation* θ , which are the natural invariants of the rotation matrix, independent from the reference frame; this frame-invariant vector has been applied to the impedance control of a three-degree-of-freedom purely rotational parallel robot (3-CPU).

If the Euler angles are used as external coordinates, the kinematics is characterized by the analytical Jacobian matrix \mathbf{J}_A ; on the contrary, using the components of the vector \mathbf{E} as external coordinates leads to the definition of the analytical Jacobian matrix \mathbf{J}_E , which tends to the geometric Jacobian matrix \mathbf{J}_G if θ tends to zero.

This important geometric property has relevant consequences on the behaviour of the resulting impedance control; to show that, the behaviours of the 3-CPU parallel robot controlled by two different impedance algorithms, based on the Jacobian matrices \mathbf{J}_A and \mathbf{J}_G , have been compared.

The simulation results show that only the geometric Jacobian-based impedance control law allows to impose properly isotropic and non-isotropic end-effector stiffness and damping; moreover, the end-effector rotations along the three principal stiffness/damping directions are almost decoupled and similar to linear

second-order systems, without the need of the model-based compensation of the inertial terms, which is computationally heavy.

For all of these reasons, using the components of the vector \mathbf{E} as external coordinates is suitable for all the applications in which a intuitive and decoupled control of the rotational compliance is required; for example, haptic human-machine interfaces for teleoperation of robots and control sticks of real or virtual aircrafts and helicopters; compliant tables for carrying parts in robotized assembly lines.

The dynamic performance of a robot controlled by the proposed algorithm depends on the inertial properties, on the features of the actuators and on the stiffness and damping matrices; adopting a proper mechanical design in combination with actuators characterized by high force/torque it is possible to impose high values of control stiffness and consequently to perform high frequency motion.

Although the main objective of impedance control is to obtain rotational compliance in one or more directions, high rotational positioning accuracy can be obtained in the remaining directions by imposing high values of the corresponding elements of the stiffness matrix; obviously, in the real implementation the maximum accuracy is limited by the mechanical stiffness and by the accuracy of the sensors.

In the following of the research, the proposed control algorithms will be experimentally tested on the 3-CPU rotational parallel robot prototype shown in Fig. 15 [29].

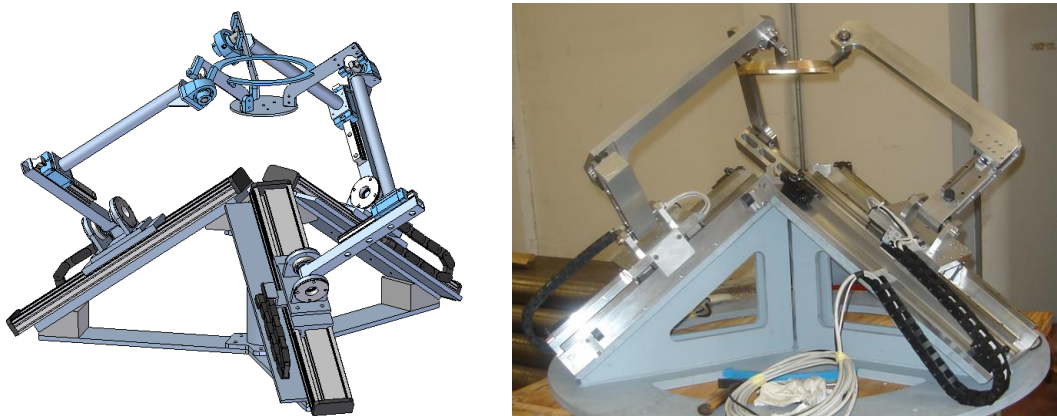


Fig. 15 – 3-CPU parallel robot prototype

REFERENCES

- [1] N.H. Raibert and J.J. Craig, "Hybrid position/force control of manipulators", ASME J. Dynamic Systems, Measurements and Control, vol. 103, pp.126-133, 1981.
- [2] N. Hogan, "Impedance control: an approach to manipulation, parts I-III", ASME J. Dynamic Systems, Measurements and Control, vol. 107, pp.1-24, 1985.
- [3] D.E. Whitney, "Historical perspective and state of the art in robot force control", Int. J. Robotics Research, vol.6, n°1, pp.3-14, 1987.
- [4] B. Siciliano, & L. Villani, Robot force control, Kluwer, 2000.
- [5] T. Yoshikawa, "Force control of robot manipulators," Proceedings of IEEE Int. Conf. on Robotics and Automation, San Francisco, USA, 2000, pp. 220–226.
- [6] L. Rey, & R. Clavel, The Delta robot: a position paper, Annals of CIRP, 47, 1998, 347-351.
- [7] V.E. Gough and S.G. Whitehall, "Universal Tyre Test Machine", in Proc. FISITA 9th Intl. Tech. Congress, May 1962, pp.117-137.
- [8] D. Stewart, A platform with six degrees of freedom, Proc. Instr. Mech. Engrs, 180-1(15), 1965, 371-386.
- [9] K.-E. Neumann, "Robot," U.S. Patent 4 732 525, 1986.
- [10] J.P. Merlet, "Force-feedback control of parallel manipulators", Proc. IEEE Int. Conf. on Robotics and Automation, Philadelphia, U.S.A., April 24-29, 1988, Vol. 3; 1484-1489.
- [11] S.M. Satya, P.M. Ferriera and M.W. Spong, "Hybrid Control of a Planar 3-Dof Parallel Manipulator for Machining Operations", Transaction of the NAMRI/SME, 1995, Vol. 23; 273-280.
- [12] M. Callegari, A. Suardi, "On the force-controlled assembly operations of a new parallel kinematics manipulator", in Proc. IEEE Mediterranean Conf. on Control and Automation, Rhodes, June 18-20, 2003, IV06-02.
- [13] F. Caccavale, B. Siciliano and L. Villani, "The Tricept Robot: Dynamics and Impedance Control", IEEE/ASME Trans. Mechatronics, Vol.8 No.2, pp.263-268, 2003.
- [14] G.M. Acaccia, L. Bruzzone, M. Callegari, R.C. Michelini, R.M. Molfino, & R.P. Razzoli, Functional assessment of the impedance controller of a parallelly actuated robotic six d.o.f. rig, Proc. 6th IEEE Mediterranean Conference on Control and Systems (MCCS), Alghero, Italy, 1998, 397-402.
- [15] E.D. Fasse, & C.M. Gosselin, On the spatial impedance control of Gough-Stewart platforms, Proc. 1998 IEEE Intl. Conference on Robotics & Automation, Leuven, Belgium, 1998, 1749-1754.
- [16] E.D. Fasse, & C.M. Gosselin, Spatio-geometric impedance control of Gough-Stewart platforms, IEEE Trans. on Robotics & Automation, 15(2), 1999, 281-288.
- [17] F. Caccavale, C. Natale, B. Siciliano, L. Villani, "Six-DOF impedance control based on angle/axis representations," IEEE Trans. on Robotics and Automation, vol. 15, pp. 289-300, 1999.
- [18] J. Angeles, Rational kinematics (New York: Springer-Verlag, 1988).
- [19] J.M. Selig, Geometric Fundamentals of robotics, Springer, 2005
- [20] F. Caccavale, B. Siciliano, & L. Villani, The role of Euler parameters in robot control, Asian J. of Control, 1(1), 1999, 25-34.
- [21] S. Chiaverini, & B. Siciliano, The Unit Quaternion: A Useful Tool for Inverse Kinematics of Robot Manipulators, Systems Analysis, Modelling and Simulation, 35, 1999, 45-60.
- [22] I. A. Bonev, & J. Ryu, A new approach to orientation workspace analysis of 6-DOF parallel manipulators, Mechanism and Machine Theory, 36(1), 2001, 15-28.
- [23] R.L. Hollis, S.E. Salcudean, & A.P. Allan, A six-degree-of-freedom magnetically levitated variable compliance fine-

- motion wrist: design, modelling and control, IEEE Trans. on Robotics and Automation, 7, 1991, 320-332.
- [24] L.E. Bruzzone, R.M. Molfino, "A geometric definition of rotational stiffness and damping applied to impedance control of parallel robots", International Journal of Robotics and Automation, Vol. 21, Issue 3, 2006, pp. 197-206.
- [25] M. Callegari, P. Marzetti, B. Olivieri: "Kinematics of a Parallel Mechanism for the Generation of Spherical Motions", in J. Lenarcic and C. Galletti (eds), On Advances in Robot Kinematics, Kluwer, 2004. pp.449-458.
- [26] T. Valency, & M. Zacksenhouse, Accuracy/Robustness Dilemma in Impedance Control, Journal of Dynamic Systems, Measurement, and Control, 125(3), 2003, 310-319.
- [27] F. Caccavale, B. Siciliano, & L. Villani, Robot Impedance Control with Nondiagonal Stiffness, IEEE Trans. on Automatic Control, 44, 1999, 1943-1946.
- [28] M. Callegari, P. Marzetti: "Inverse Dynamics Model of a Parallel Orienting Device", Proc. 8th International IFAC Symposium on Robot Control: SYROCO 2006, Bologna, 6-8 September 2006.
- [29] M. Callegari: "Design and Prototyping of a SPM Based on 3-CPU Kinematics", In: Parallel Manipulators, New Developments, Aleksandar Lazinica ed., ARS publ. Vienna, Apr. 2008. (available on-line at <http://books.i-techonline.com/>)